Journal of Non-Crystalline Solids 404 (2014) 104–108

Contents lists available at ScienceDirect

Journal of Non-Crystalline Solids

journal homepage: www.elsevier.com/ locate/ jnoncrysol

The structural role of Ti in a thermally-treated $Li_2O - B_2O_3–Al_2O_3$ glass system

V.A. Silva [a,d,*], M.L.F. Nascimento [b,c], P.C. Morais [d,e], N.O. Dantas [a]

[a] Laboratório de Novos Materiais Isolantes e Semicondutores (LNMIS), Institute of Physics, Federal University of Uberlândia, Uberlândia MG38400-902, Brazil
[b] Vitreous Materials Laboratory, Institute of Humanities, Arts and Sciences, Federal University of Bahia, Ondina University Campus, Salvador BA 40170-115, Brazil
[c] PROTEC/PEI—Postgraduate Program in Industrial Engineering, Department of Chemical Engineering, Polytechnic School, Federal University of Bahia, Salvador BA 40210-630, Brazil
[d] Núcleo de Física Aplicada, Institute of Physics, University of Brasília, Brasília DF 70910-900, Brazil
[e] Huazhong University of Science and Technology, School of Automation, Wuhan 430074, China

ARTICLE INFO

Article history:
Received 16 May 2014
Received in revised form 23 July 2014
Available online 23 August 2014

Keywords:
Crystallization;
Glass-ceramic;
TiO_2

ABSTRACT

A 50**Li**$_2$O·45**B**$_2$O$_3$5**Al**$_2$O$_3$ (**LBA**, in mol%) glass matrix doped with increasing TiO_2 content was synthesized and its physical properties were investigated by differential thermal analysis (DTA), X-ray diffraction (XRD), and Raman spectroscopy. The thermograms showed typical vitreous curves with two clear crystallization peaks that are related to major crystalline phases in this glass system and in agreement with XRD results. The higher temperature crystallization peak (T_{C2}) shifted towards the lower temperature peak (T_{C1}) as TiO_2 content increased. After specific heat treatments, the XRD measurements revealed the α-$LiBO_2$, γ-$LiAlO_2$ and $LiTiO_2$ crystalline phase formations and the predominance of the first phase. The γ-$LiTiO_2$ phase was particularly responsible for the variation in the second peak crystallization kinetics. In addition, crystal growth phase competition between γ-$LiAlO_2$ and $LiTiO_2$ occurred as TiO_2 content increased; however, the main α-$LiBO_2$ phase did not change. Raman spectra showed typical phonon modes associated with crystalline phases observed in XRD and main phases observed in DTA. Phonon modes were also associated with the $LiTiO_2$ crystalline phase that was first observed in the glassy matrix.

1. Introduction

Borate glasses (B_2O_3-based) have been widely investigated for potential applications in optical devices [1,2]. Optical transparency in the visible and near infrared wavelengths is the key property of these glasses. Additionally, diboron trioxide (B_2O_3) is a typical (par excellence) glass forming material with a relatively low melting point that facilitates production and reduces costs. Applications for B_2O_3-based glasses can be expanded by adding alkali metals and alkaline earth metal oxides that enhance physicochemical properties, such as moisture resistance, compared to pure borate glasses [3]. In particular, the addition of Li_2O enhances the devitrification of B_2O_3-based glasses, which permits synthesis of Li_2O-based vitroceramics [4]. Actually, the ratio between B_2O_3 (network-forming) and Li_2O (network-modifying) content dictates the applications of the $Li_2O–B_2O_3$ glass system [5–8]. Al_2O_3 co-doping with the $Li_2O–B_2O_3$ glass system is an additional synthesis strategy that enhances chemical stability and allows tuning of the end glass properties for technological applications. The crystallization kinetics of this new Lithium–Boron–Aluminum (LBA) glass system ($Li_2O–B_2O_3–Al_2O_3$) were recently reported [3]. Furthermore, TiO_2 has been added to several glass systems for applications in non-linear optics [9] and to better understand its influence as a nucleating agent on crystallization kinetics [10]. However, little work has been done on how Ti-ions influence the formation of crystalline phases during the devitrification of B_2O_3-based glasses. In this study, crystallization of a LBA:Ti glass system was controlled and its thermal, structural and optical properties were comparatively investigated by differential thermal analysis (DTA), X-ray diffraction (XRD), and Raman spectroscopy (RS).

2. Experimental procedure

The **LBA** glass matrix with nominal composition of 50**Li**$_2$O·45**B**$_2$O$_3$·5**Al**$_2$O$_3$ (mol%) doped with 0, 0.5, 1.0, …, 5.0 TiO_2 (wt.%) was prepared by mixing the correct proportion of high grade chemicals and synthesizing by fusion at 1000 °C for 10 min in porcelain crucibles under ambient atmosphere. Afterwards, the melt was rapidly cooled (in air) and compressed into 2 mm thick molds between two brass plates (previously cooled to 0 °C). The glass block was then hammered into pieces that were further milled and pulverized to within the desired grain range. Finally, the glass powder was sieved through a 53–212 μm polymer mesh for DTA, XRD, and Raman analysis.

Thermal characterizations were performed using a Shimadzu DTA-50 system operating at a 20 °C/min heating rate and in a nitrogen atmosphere (with 50 mL/min flux). Each run used 40 mg powder samples in

* Corresponding author at: Núcleo de Física Aplicada, Institute of Physics, University of Brasília, Brasília DF 70910-900, Brazil.
E-mail address: valdeir@fis.unb.br (V.A. Silva).

http://dx.doi.org/10.1016/j.jnoncrysol.2014.07.046
0022-3093/

alumina crucibles. Characteristic temperatures were determined by the "Tangent Method" which entails setting base-lines before and after each event observed in the DTA thermograms and then extending the base lines until they intersect at a point corresponding to the determined temperature. Based on the DTA results, the samples were heated at the maximum crystallization temperature (T_{C1} or T_{C2}) for 10 min. X-ray diffractograms were recorded using a Rigaku Ultima IV (operating at 35 kV, 15 mA, and $\lambda = 1.54056$ Å $CuK_{\alpha 1}$ wavelength) with 2θ scans from 10° to 60° and step increments of 0.050° lasting 10 s each. Room temperature Raman spectra were obtained with a Jobin-Yvon model T64000 operating with 1800 line/mm grades, equipped with a 2048 × 512 pixel CCD detector, and using a 514.5 nm Argon-ion laser line to illuminate the samples.

Table 1
Characteristic temperatures of LBA ±2 °C doped with increasing titania content.

TiO_2 (wt.%)	T_g	T_{X1}	T_{C1}	T_{X2}	T_{C2}
0	414.0	550.2	576.1	610.6	625.5
0.5	409.0	537.3	564.8	604.8	624.7
1.0	412.2	544.1	569.8	606.8	625.5
1.5	410.8	538.0	564.1	604.6	623.4
2.0	411.3	545.3	573.0	608.3	624.6
2.5	415.1	555.7	583.6	607.8	619.1
3.0	412.7	552.6	583.7	607.6	618.3
3.5	414.7	545.1	581.1	604.4	612.6
4.0	413.0	550.6	580.2	–	612.4
4.5	414.6	548.3	572.0	–	–
5.0	413.0	545.2	566.0	–	–

3. Results and discussions

Fig. 1 shows the thermograms of the as-synthesized undoped (nominal $x = 0$) and the doped (nominal $0.5 \le x \le 5.0$) LBA glass matrices without further heat treatment. The synthesized LBA glass matrix presents two characteristic crystallization peaks (T_{C1} and T_{C2}). The glass transition temperature (T_g) and the crystallization peak maxima (T_{C1} and T_{C2}) are indicated in the lower part of Fig. 1. Table 1 shows the characteristic temperatures in the entire range of the x nominal values ($0.0 \le x \le 5.0$). The thermograms in Fig. 1 and the corresponding data in Table 1 show that: (*i*) there is no significant change in T_g as TiO_2 is added into the initial synthesis mixture; and (*ii*) as greater quantities of TiO_2 are added, the second crystallization peak (T_{C2}) shifts to lower temperatures and eventually merges with the first crystallization peak (T_{C1}). This result indicates a competition between the different phases

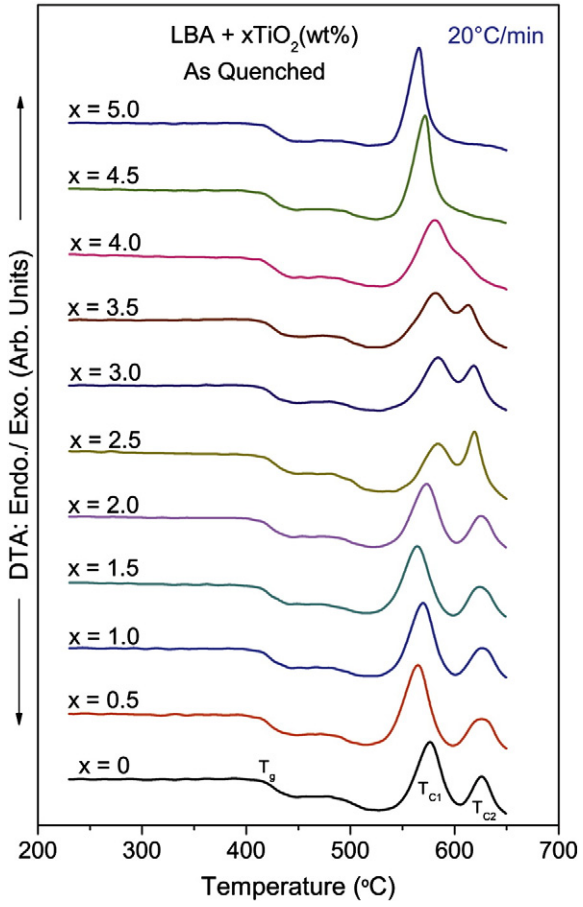

Fig. 1. Thermograms (DTA) of the LBA glass matrix ($x = 0$) and doped compositions without further heat treatment. The heat rate was fixed at 20 °C/min. Note that $T_{C2} \rightarrow T_{C1}$ with higher titania (x) content.

formed during the first and second crystallizations. Additionally, at higher TiO_2 concentrations ($x = 4.5$ and 5.0 wt.%) the crystallization peaks are indistinguishable and therefore labeled as T_{C1} (see Table 1).

It should be noted that titanium oxide is considered a nucleating agent of crystallization in amorphous materials, which would explain some of the crystallization peaks. In fact, small quantities of TiO_2 in the glass matrices appear to enhance the forming capacity and chemical durability of the glass [9]. In general, titanium ions exist as Ti^{4+} in the glass network and participate in the glass-forming network with TiO_4, TiO_6 and sometimes TiO_5 (composed of trigonal bipyramids) structural units [11,12]. Titanium and aluminum can replace some glass former structures, but do not readily form glasses by themselves. Thus, they are considered *intermediate* in behavior between glass formers (e.g. boron oxide unities) and modifiers (e.g. lithium oxide). One should argue that from such observation it is possible to assess the information of why T_g did not change with the increasing titanium content. However, the observed T_g value versus titania content showed in Fig. 1 and also in Table 1 could be correlated to phase separation. One reason could be related to a second down shift between T_g and T_X values. It is important to point out that alkali aluminoborate glass structures are not well understood up to now [13], with few reported studies [14,15]. In particular, the sample under study is at the border of the glass formation region observed by Kim and Hummel [14], with composition similar to the metaborate glass [16].

Fig. 2 shows the Raman spectra of the as-synthesized samples without any further heat treatment that correspond to the samples in Fig. 1. Notice that the undoped sample (nominal $x = 0$) presents four main bands with peaks at 450, 737, 766, and 970 cm^{-1}. Borate glasses are formed via structural units such as boroxol rings, diborate groups, and chain-type metaborate groups [17–19]. According to the literature, the Raman band near 450 cm^{-1} is related to the presence of B–O–B stretching vibrations from the BO_4 units [20]. The Raman mode peaks at 737 and 766 cm^{-1} are due to the out-of-plane bending mode associated with metaborate triangles [18] whereas the Raman band near 970 cm^{-1} is related to the symmetric stretching mode of the B(3)–O bonds [21]. Fig. 2 also shows that two new Raman bands emerge as TiO_2 content increases in the LBA glass matrix: (*i*) the first centered at 309 cm^{-1} and (*ii*) the second at about 866 cm^{-1}. The intensities of the two emerging Raman modes rise steeply as titanium-doping increases and can be attributed to Ti–O bonds (309 cm^{-1}) and the BO_4^- group (866 cm^{-1}) [22].

Fig. 3 presents the X-ray diffractograms of the as-synthesized LBA-based glass samples after thermal treatment at T_{C1} for 10 min and shows no evidence of crystalline $Li_3AlB_2O_6$ phase formation. Nevertheless, we found evidence of the crystalline α-$LiBO_2$ phase and other unidentified lower-content crystalline phases. A previous study reported crystalline phase formation when the LBA glass matrix was heat treated at T_X (the onset crystallization temperature) [3]. According to Dantas et al. [3], the crystalline phases $Li_3AlB_2O_6$ (PDF: 01-072-4641, 01-073-7384) [15] and α-$LiBO_2$ (PDF: 01-072-1087,84-118, 01-076-2212)

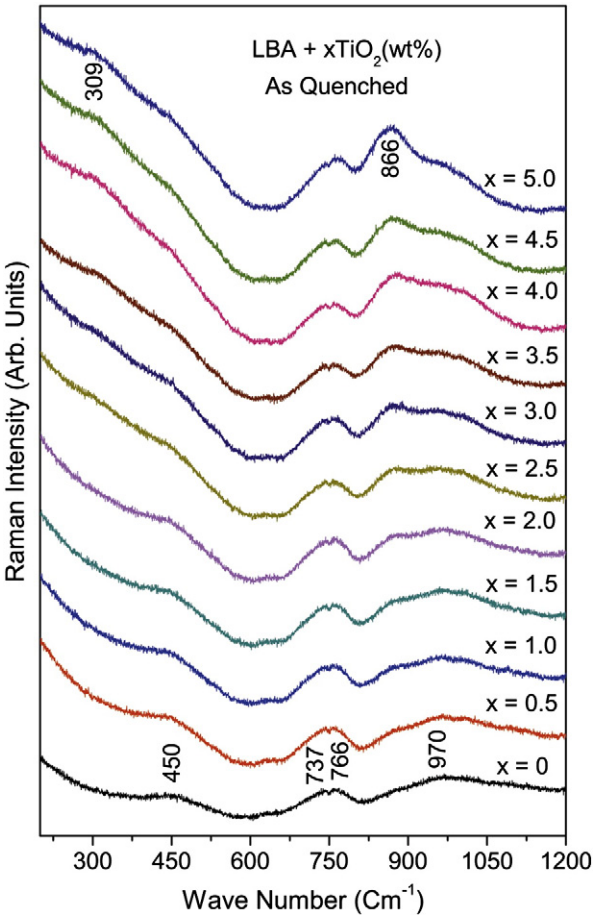

Fig. 2. Room temperature Raman spectra of the LBA glass matrix ($x = 0$) and doped compositions without further heat treatment.

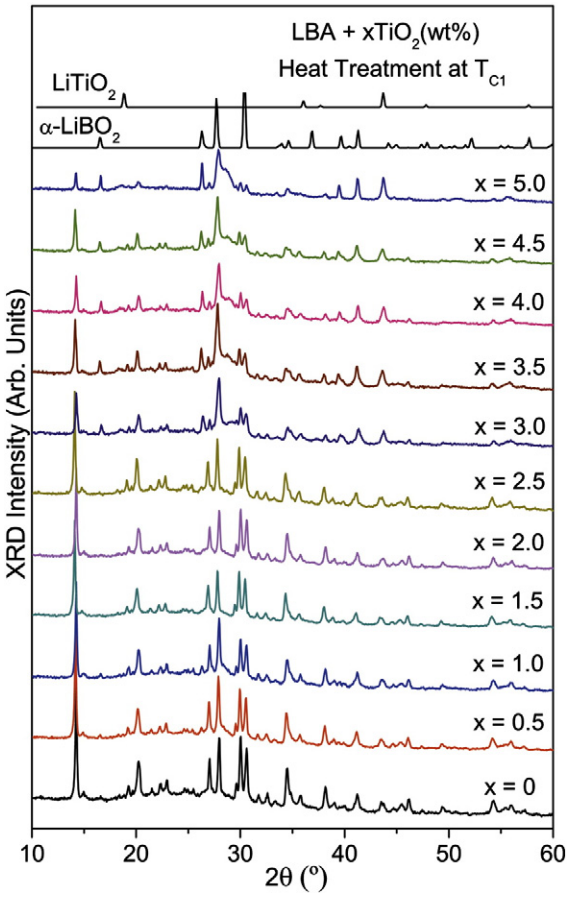

Fig. 3. Diffractograms (XRD) of the heat-treated LBA glass matrix ($x = 0$) plus titania-doped content at T_{C1} during 10 min.

[23] were observed after thermal treatment at T_X for 1–7 h. Chryssikos et al. [16] also noted that crystallization is strongly dependent on thermal treatment conditions. Samples thermally treated at T_{C2} (Fig. 4) show α-$LiBO_2$ as the major phase and competition between the other two crystalline phases: γ-$LiAlO_2$ (PDF: 01-075-0905,38-1464) [24] and $LiTiO_2$ (PDF: 77-1389) [25], identified by asterisks (*) in the $x =$ 2.5 diffractogram. Fig. 4 shows that the diffraction peak at 22.51° almost disappears and the intensity of the diffraction peak at 18.46° rises when x increases from 2.5 to 4.0. The γ-$LiAlO_2$ phase presents tetrahedral coordination with oxygen at the vertices (fourth coordination) and lithium or aluminum at the center whereas the $LiTiO_2$ phase presents octahedral coordination (sixth coordination) with oxygen at the vertices and lithium and titanium atoms at the center. Thus, the LBA glass matrix is oxygen rich, which favors the $LiTiO_2$ phase. At this point we claim that Ti-ions may replace Al-ions in the thermally treated Ti-doped LBA glass matrix because of similarities in ionic radii and valence. This conclusion accounts for the presence of the two concurrent crystalline phases $LiTiO_2$–γ-$LiAlO_2$ observed in the diffractograms (Fig. 4) and agrees with previous thermal results where T_g did not change with increasing titania content.

Fig. 5 summarizes the competition between the crystalline α-$LiBO_2$–$LiTiO_2$–γ-$LiAlO_2$ phases of the samples thermally treated at T_{C2}. To study the competition among the major phases associated with the diffraction peaks in Fig. 5, we obtained the average crystal size $d_{crystal}$ from the Debye–Scherrer equation [26]:

$$d_{crystal} = \frac{0.9\lambda}{(w)\cos(\theta_B)} \quad (1)$$

where λ is the X-ray wavelength, θ_B is the Bragg's angle and w is the full-width at half maximum, taking into account the instrumental line broadening [27].

The XRD data show little variation in the average α-$LiBO_2$ crystal size (the predominant phase). This result could be parallel with the glass transition temperature results. It is important to point out that, even considering error bars, the average crystal size of the α-$LiBO_2$ crystalline phase has roughly the same trend as the measured T_g values collected in Table 1. The reason is that the lithium borate crystals grow from the predominant glass phase with similar composition. In other words, while increasing the titania content there is no clear tendency to decrease or increase the average lithium borate crystal size as observed in the behavior of major glass phases (indicated by T_g measurements). In opposition to this, a competition between the two other identified crystalline phases, which are minorities in the glass composition is observed. In other words, there is a competition between the average crystal sizes of the $LiTiO_2$ and γ-$LiAlO_2$ phases as TiO_2 content increases. Actually, we found that the average crystal size of γ-$LiAlO_2$ decreases whereas the average crystal size of $LiTiO_2$ increases with TiO_2 addition.

Fig. 6 presents the room temperature Raman spectra of the Ti-undoped ($x = 0$) and Ti-doped ($x = 4.0$) LBA glass samples thermally treated at T_{C2}. A detailed fitting of the Raman data of the Ti-undoped sample (Fig. 6a) reveals α-$LiBO_2$ and γ-$LiAlO_2$ crystalline phases. These results are in agreement with the DRX data reported in the literature [16] and the crystallization peaks determined by thermal analysis. However, Raman data fitting for the Ti-doped sample (Fig. 6b) reveals the $LiTiO_2$ crystalline phase. As far as we know, this is the first report of Raman modes of the $LiTiO_2$ crystalline phase in a glass matrix. Note that the Raman band peaks at 309 and 866 cm^{-1} in the LBA glass

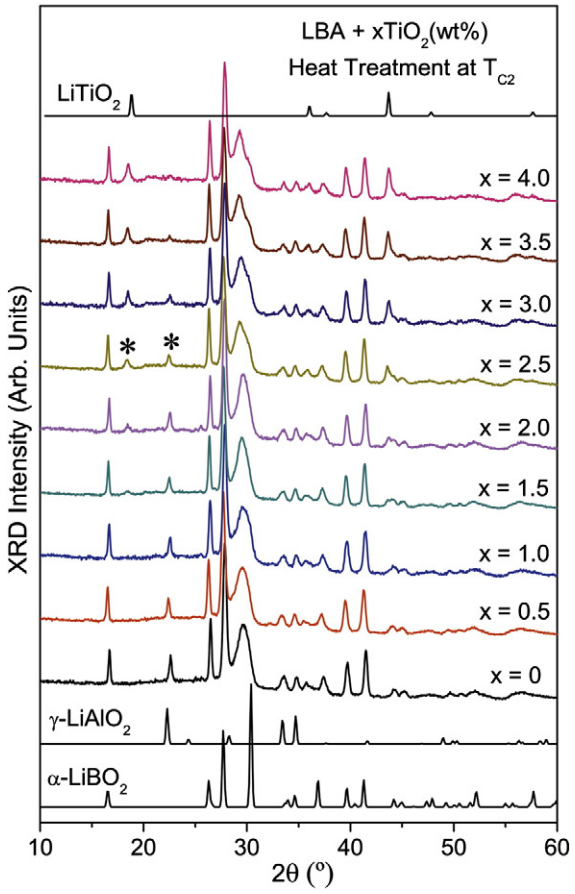

Fig. 4. Diffractograms (XRD) of the heat-treated LBA glass matrix plus titania-doped content at T_{C2} during 10 min. Asterisks (*) indicate a γ-$LiAlO_2$ iTiO_2 competition.

samples (without heat treatment) were indeed observed in the heat-treated samples.

4. Conclusions

We have combined DTA, XRD and Raman techniques to provide a detailed description of the structural role played by Ti-ions in a thermally-treated LBA glass matrix. Differential thermal analysis, which probes thermally-activated processes, identified the glass transition temperature (T_g) and two crystallization peaks (T_{C1} and T_{C2}). Increasing additions of TiO_2 shifted the second crystallization peak (T_{C2}) to lower temperatures until it merged with the first (T_{C1}). This result indicates a competition between the phases formed during the first and the second crystallizations. XRD measurements showed the primary (α-$LiBO_2$) and secondary (γ-$LiAlO_2$, $LiTiO_2$) crystalline phases. The competition suggested by DTA was clarified by XRD. In fact, because of its lower formation energy, the $LiTiO_2$ phase replaces the γ-$LiAlO_2$ phase, which shifts T_{C2} to lower values as Ti concentration increases. The Raman spectra showed α-$LiBO_2$, γ-$LiAlO_2$ and $LiTiO_2$ crystalline phases and confirmed the observations from the DRX data. Detailed analysis showed that crystallization kinetics are faster and highly dependent on heat treatment conditions. Finally, as far as we know this is the first report showing Raman modes of the crystalline $LiTiO_2$ phase in a glass matrix.

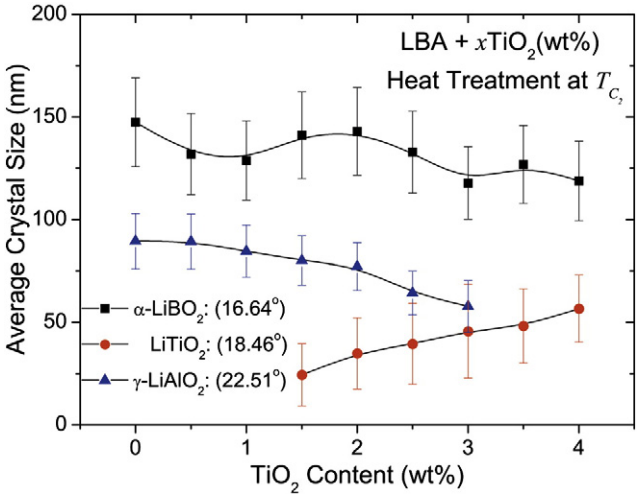

Fig. 5. Average crystal size as a function of titania content for samples heat-treated at T_{C2} for 10 min. Phases are identified by their characteristic XRD peaks shown in previous figures. Solid lines are only visualization aides.

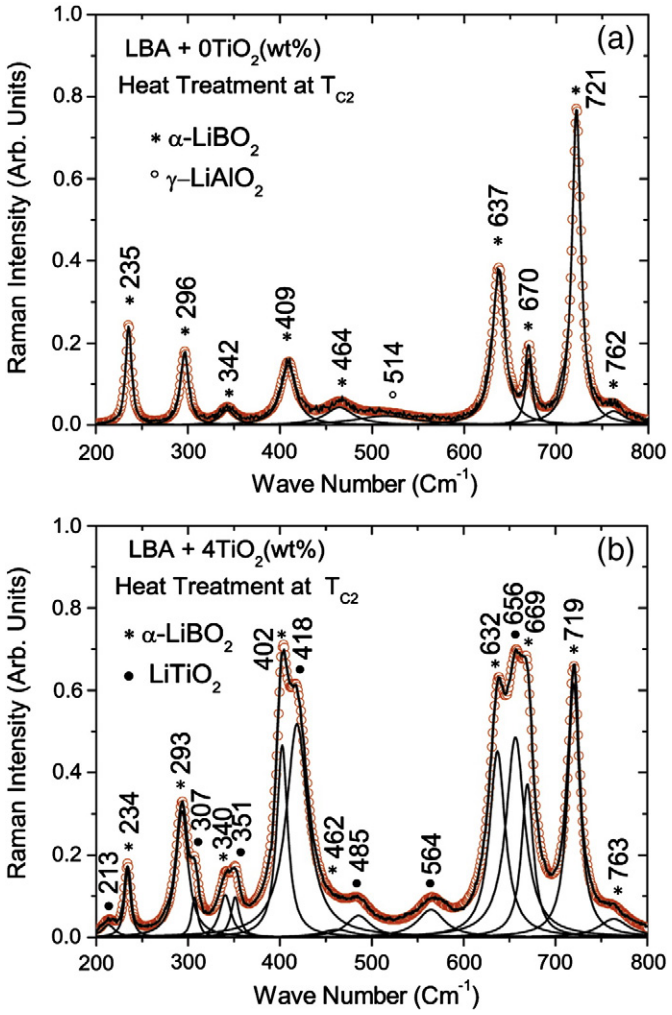

Fig. 6. Detailed Raman fittings for samples heat-treated at T_{C2}; $x = 0$ (*a*) and $x = 4$ (*b*).

Acknowledgments

The authors are grateful for the financial support from the following Brazilian agencies: CNPq (306178/2011-7, 305373/2009-9), CAPES (PEI-11/2009) and FAPEMIG (APQ-01838-12) and for XRD measurements from the laboratory of Prof. Edi M. Guimarães at the Universidade de Brasília (Brazil).

References

[1] A.R. Devi, C.K. Jayasankar, Mater. Chem. Phys. 42 (1995) 106.
[2] M. Abdel-Baki, F. El-Diasty, J. Solid State Chem. 184 (2011) 2762.
[3] N.O. Dantas, V.A. Silva, O.O.D. Neto, M.L.F. Nascimento, Braz. J. Phys. 42 (2012) 347.
[4] J. Zarzycki, Glasses and the Vitreous State, University Press, Cambridge, 1991.
[5] T. Hasegawa, J. Non-Cryst. Solids 357 (2011) 2857.
[6] N. Sdiri, H. Elhouichet, M. Ferid, J. Non-Cryst. Solids 389 (2014) 38.
[7] P. Riello, P. Canton, N. Comelato, S. Polizzi, M. Verità, G. Fagherazzi, H. Hofmeister, S. Hopfe, J. Non-Cryst. Solids 288 (2001) 127.
[8] M. Rathore, A. Dlavi, J. Non-Cryst. Solids 402 (2014) 79.
[9] L. Koudelka, P. Mošner, M. Zeyer, C. Jäger, J. Non-Cryst. Solids 326 (2003) 72.
[10] R. Balaji Rao, D. Krishna Rao, N. Veeraiah, Mater. Chem. Phys. 87 (2004) 357.
[11] N. Shimoji, T. Hashimoto, H. Nasu, K. Kamiya, J. Non-Cryst. Solids 324 (2003) 50.
[12] A. Shaim, M. Et-tabirou, J. Mater. Chem. Phys. 80 (2003) 63.
[13] J.E. Shelby, Introduction to glass science and technology, R. Soc. Chem. (2005) 98–99.
[14] K.H. Kim, F.A. Hummel, J. Am. Ceram. Soc. 45 (1962) 487.
[15] M. He, X.L. Chen, B.Q. Hu, T. Zhou, Y.P. Xu, T. Xu, J. Solid State Chem. 165 (2002) 187.
[16] G.D. Chryssikos, E.I. Kamitsos, A.P. Patsis, M.S. Bitsis, M.A. Karakassides, J. Non-Cryst. Solids 126 (1990) 42.
[17] W.L. Konijnendijk, J.M. Stevels, J. Non-Cryst. Solids 18 (1975) 307.
[18] G.D. Chryssikos, M.S. Bitsis, J.A. Kapoutsis, E.I. Kamitsos, J. Non-Cryst. Solids 217 (1997) 278.
[19] A.A. Osipov, L.M. Osipova, J. Phys. Chem. Solids 74 (2013) 971.
[20] R.K. Brow, D.R. Tallant, G.L. Turner, J. Am. Soc. 80 (1997) 1239.
[21] Y. Yu, J.-H. Yu, G. Xiong, C. Li, F.-S. Xiao, Phys. Chem. Chem. Phys. 3 (2001) 2692.
[22] N.C.A. de Sousa, M.T. de Araujo, C. Jacinto, M.V.D. Vermelho, N.O. Dantas, C.C. Santos, I. Guedes, J. Solid State Chem. 184 (2011) 3062.
[23] G. Will, A. Kirfel, B. Josten, J. Less-Common Met. 2 (1981) 255.
[24] M. Marezio, J.P. Remeika, J. Chem. Phys. 44 (1966) 3348.
[25] R.J. Cava, D.W. Murphy, S. Zahurak, J. Solid State Chem. 53 (1984) 64.
[26] P. Scherrer, Nachrichten Gesell, Wiss. Göttingen 26 (1918) 98.
[27] P. Thompson, D.E. Cox, J.B. Hastings, J. Appl. Cryst. 20 (1987) 79.